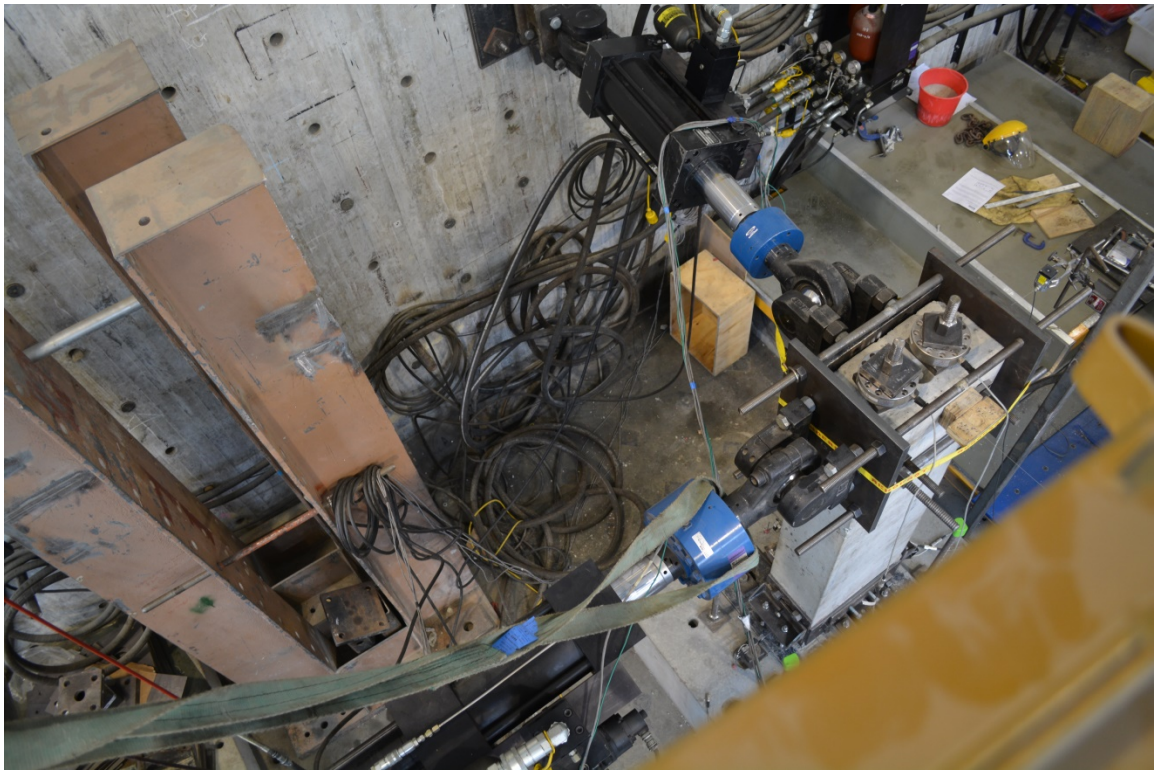

Improving multi-axial hybrid testing capability to replicate earthquake actions on structures

THE UNIVERSITY OF AUCKLAND
NEW ZEALAND
Te Whare Wānanga o Tāmaki Makaurau

Ref: 3700954

July 2015

Prepared by: Mr. Ronald Gultom (PhD candidate)
Dr. Quincy Ma (Lecturer)
Department of Civil and Environmental Engineering
The University of Auckland
Private Bag 92019, Auckland Mail Centre Auckland 1142

Revision History

Revision Number	Date of Issue	Report status
1	3 July 2015	Issued to EQC

Cover photo: A photograph of the test rig for this research project

Executive Summary

This report presents the results from an experimental programme aimed to improve the pseudodynamic testing method for simulating earthquake loads on structural specimens. Specific extension of the research included developing advanced multiple actuators control to simulate multi-axial and coupled earthquake excitations. A low-damage rocking concrete column was selected as the experimental specimen and was tested pseudostatically and pseudodynamically. This allowed multiple tests on the same specimen. A sophisticated algorithm precisely applied the loads to the top of the column in two orthogonal directions through two computer controlled actuators. An additional novelty of the research was the examination of the effects of different displacement patterns and loading sequences on the column response, and the corresponding implications for laboratory testing procedures on design. Pseudostatic test results showed that different loading patterns indeed produced very different strength prediction as well as different energy dissipation characteristics. This confirmed the need to consider and intelligently select appropriate loading protocols in laboratory test, to replicate structural behaviour expected during actual seismic events. This project also found that different loading sequences within loading substeps in a pseudodynamic test can lead to different displacement responses from identical earthquake input.

Table of Contents

Revision History i
Executive Summary ii
Table of Contents iii
List of Figures iii
List of Tables iv
1.0 Introduction / Background 1
2.0 Research objectives 2
3.0 Planar Actuator Control Algorithm 3
4.0 Methodology 7
4.1 Testing Matrix 8
4.2 Prototype Structure and the Test Specimen 9
5.0 Results 13
5.1 Pseudostatic Test (Test Series A) Results 13
5.2 PSD Test (Test Series B) Results 16
6.0 Conclusion 21
Publications from this project 21
Acknowledgement 21
References 22
Appendix A - Schematic drawing, test setup, and components 23

List of Figures

Figure 2-1 Plausible displacement paths for applying an in-plane displacement 2
Figure 3-1 Position error due to actuator arching motion 3
Figure 3-2 Plan view of general initial test setup 3
Figure 3-3 A typical displaced position 4
Figure 4-1 Displacement patterns for the pseudostatic experiment 7
Figure 4-2 Spectral accelerations of the scaled earthquake records used in the testing regime 8
Figure 4-3 Prototype bridge system 9
Figure 4-4 Elevation view of test setup, stronger axis face (left) and weaker axis face (right) 10
Figure 4-5 Photographs showing the construction sequence of the unbonded PT column 11
Figure 4-6 Photographs showing the column foundation construction sequence 12
Figure 5-1 Pseudostatic force-displacement response of the column under different loading patterns (Note. QS - Circular pattern results have not been analysed) 14

Figure 5-2 Pseudostatic force-displacement envelope of the column under different loading patterns 15
Figure 5-3 PT force-displacement history under different loading patterns 15
Figure 5-4 Displacement time history and force-displacement response from PSD EQ A (Tabas) test 17
Figure 5-5 Top of column displacement during PSD EQ A (Tabas) viewed in plan 17
Figure 5-6 Displacement time history and force-displacement response from PSD EQ B (Duzce) test 18
Figure 5-7 Top of column displacement during PSD EQ B (Duzce) viewed in plan 18
Figure 5-8 Displacement time history and force-displacement response from 1999 Yarimca earthquake 19
Figure 5-9 Top of column displacement during PSD EQ F (Yarimca) viewed in plan 19
Figure 5-10 Peak displacement amplitudes during PSD EQ B (Duzce) simulation 20
Figure 5-11 Distribution of normalised amplitude errors from the PSD simulations 20
Figure A-1 Schematic drawing of column specimen 23
Figure A-2 Schematic drawing of foundation block 24
Figure A-3 Plan view of test setup 25
Figure A-4 Elevation view of test setup 26
Figure A-5 Schematic of the column with steel base plate, EMD and actuator mounts. 27
Figure A-6 Externally mounted dissipator (EMD) 28

List of Tables

Table 4-1 Experiment matrix 8
Table 4-2 Seismic hazard parameters 10
Table 4-3 Properties of prototype and model of bridge pier 10
Table 5-1 Equivalent viscous damping based on pseudostatic tests under different loading patterns .. 14

1.0 Introduction / Background

There are a number of techniques for predicting the response of structures in earthquakes. Numerical dynamic simulations are increasingly popular and they are capable of modelling many complex local and global behaviours. Despite this, there are still situations where the structural response cannot be reliably predicted and physical experimentation remains the only dependable technique for gaining insights. Moreover, numerical simulation tools are typically developed based on data acquired through experiments or they require parameters that are established through physical testing. The advancement of numerical simulation tools is therefore linked to advances in physical experimentations.

The shake table test has long been regarded as the most accurate method to replicate the response of structures during earthquakes. A shake table test directly imparts a sequence of ground displacements at the base of a specimen in real time. The shake table motion can originate from accelerations recorded during real earthquakes or generated by artificial means. A shake table test intuitively triggers dynamic behaviour of the structure (e.g. inertia and damping forces), which in turn directly replicates damage in the specimen. However, limited size and capacity of shake table restrict the size of model that can be tested. Concurrently, the cost of a large shake table and its running cost make shake table tests prohibitive. For these reasons, shake table tests are commonly performed on scaled models. This presents additional difficulties in translating results from scaled shake table tests to the expected response of the full scale prototype. The influence of size on structural characteristics can be clearly observed in reinforced concrete structures, where shear strength is greatly influenced by the size of the member and this cannot be captured when using small scale beams [1].

These challenges led to the development of the pseudodynamic test (PSD) method. This method combines the use of a numerical model and physical testing, and it permits the application of large loads to large specimen at pseudostatic rate to obtain dynamic response. This method was first implemented in Japan $ca.1975$ [2], referred to as “online testing”, and has been intensively developed there and also in the US since [3]. Today, this method has also gained popularity in worldwide, most notably the European Laboratory for Structural Assessment (ELSA) at Ispra, Italy [4], in addition to several universities and research institutes in China and Taiwan [5, 6].

Past research comparing the pseudostatic, dynamic and pseudodynamic tests have been restricted to uni-directional ground motions in the main. In reality, earthquakes produce complex, multi-directional excitations and most buildings are irregular both in plan and vertically. These make it ever more important to investigate the test accuracy when attempting to simulate coupled multiaxial response.

2.0 Research objectives

This research project makes use of two dynamic servo-hydraulic actuators with ±300 kN load capacity and ±150 mm stroke located at the University of Auckland structural testing laboratory [7]. More information about the facility is summarised in a paper by the authors [8]. The current research follows the work from the aforementioned paper which developed a novel actuator delay compensation method to conduct PSD continuously (without stoppages) at increased loading rate The PSD tests at the University of Auckland have so far been restricted to unidirectional excitations. This project aims to extend Auckland's PSD setup capability to allow multi-axial PSD tests.

In experimental testing, there are an infinite number of possible load paths to apply deformations in three dimensional space to a specimen. For example, consider a reinforced concrete column with rectangular cross-section subjected to a displacement from Point 1 to Point 2 as shown in Figure 2-1. There are three convenient and plausible paths to command the actuators to displace the section. For asymmetrical section, where section stiffness are different in the two principal directions, different loading sequences will lead to different strength degradation, stiffness degradations and energy dissipation characteristics. This was demonstrated in a previous study where a rectangular hollow steel columns was tested using various predefined displacement patterns and the behaviour of the column in the inelastic range was shown to be path-sensitive [9].

There are therefore two main objectives of the experiments reported herein, these are,

- to set up a biaxial PSD testing facility at the University of Auckland structural testing laboratory to enable more realistic simulations of earthquake load; and
- to investigate the effect of different displacement paths and loading sequences on energy dissipation of inelastic structures and accuracies of the biaxial PSD tests.

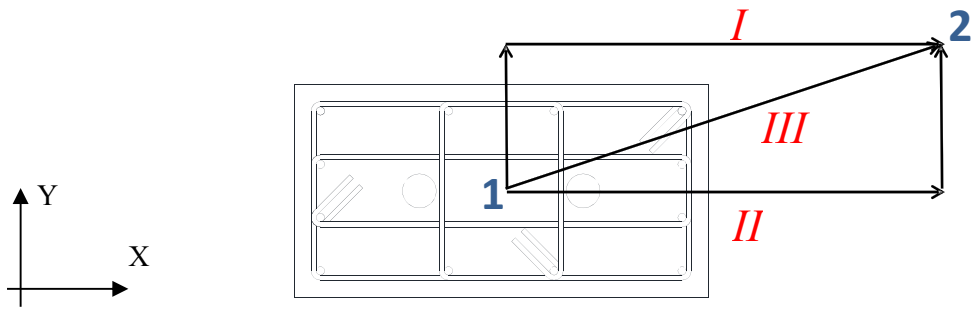

Figure 2-1 Plausible displacement paths for applying an in-plane displacement

3.0 Planar Actuator Control Algorithm

Precise control of structural test specimen displacement in a two dimensional plane is more complex than it may first appear. This is typically achieved by controlling the lengths of two or more perpendicularly placed hydraulic actuators connected to the specimen. The control of the specimen location thus involves nonlinear geometric interactions of the actuators. This is illustrated by an example of arching motion consideration in Figure 3-1.

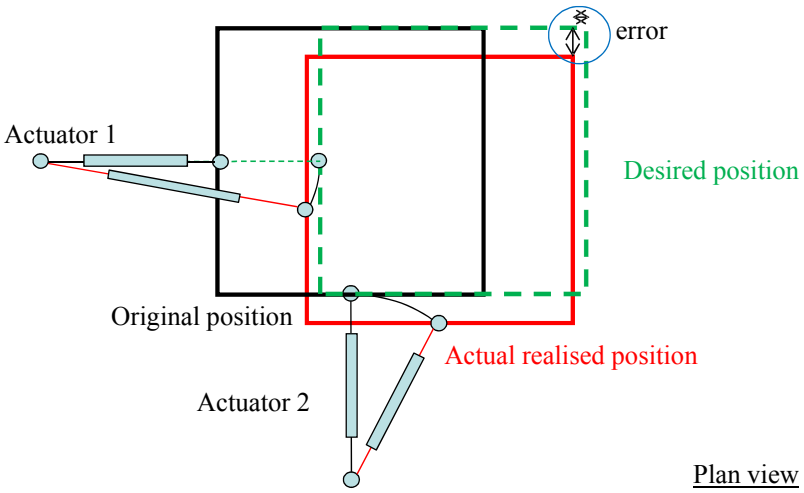

Figure 3-1 Position error due to actuator arching motion

This project developed a non-linear transformation and tracking algorithm that ensures specimen deformations are applied precisely in real time. Consider the plan view of the initial setup of a PSD test in Figure 3-2.

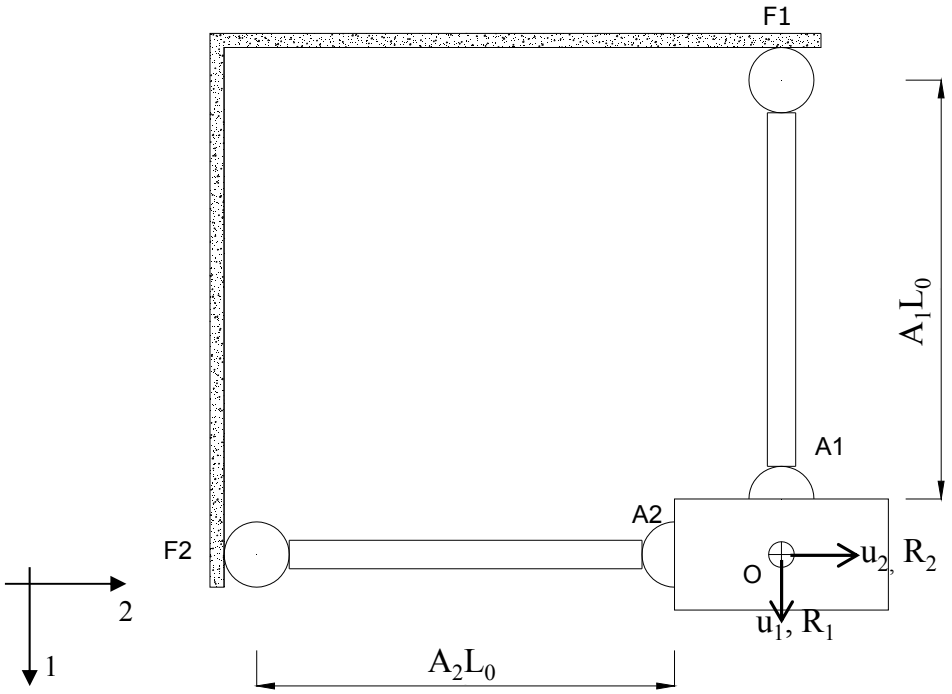

Figure 3-2 Plan view of general initial test setup

The variables in Figure 3-2 are described below.

A_1L_0 : initial length of Actuator 1
A_2L_0 : initial length of Actuator 2
O : initial position of the column geometric centre
u_1, R_1 : displacement and restoring force in the *1* direction
u_2, R_2 : displacement and restoring force in the *2* direction
A1, F1 : end nodes of Actuator 1
A2, F2 : end nodes of Actuator 2

The initial lengths of the actuators (A_1L_0 and A_2L_0) do not change throughout an experiment and can be determined at the beginning of a test. O is located at the specimen's geometric centre. Only two translational degree-of-freedom (DOFs) are considered in these experiments; torsional response is neglected.

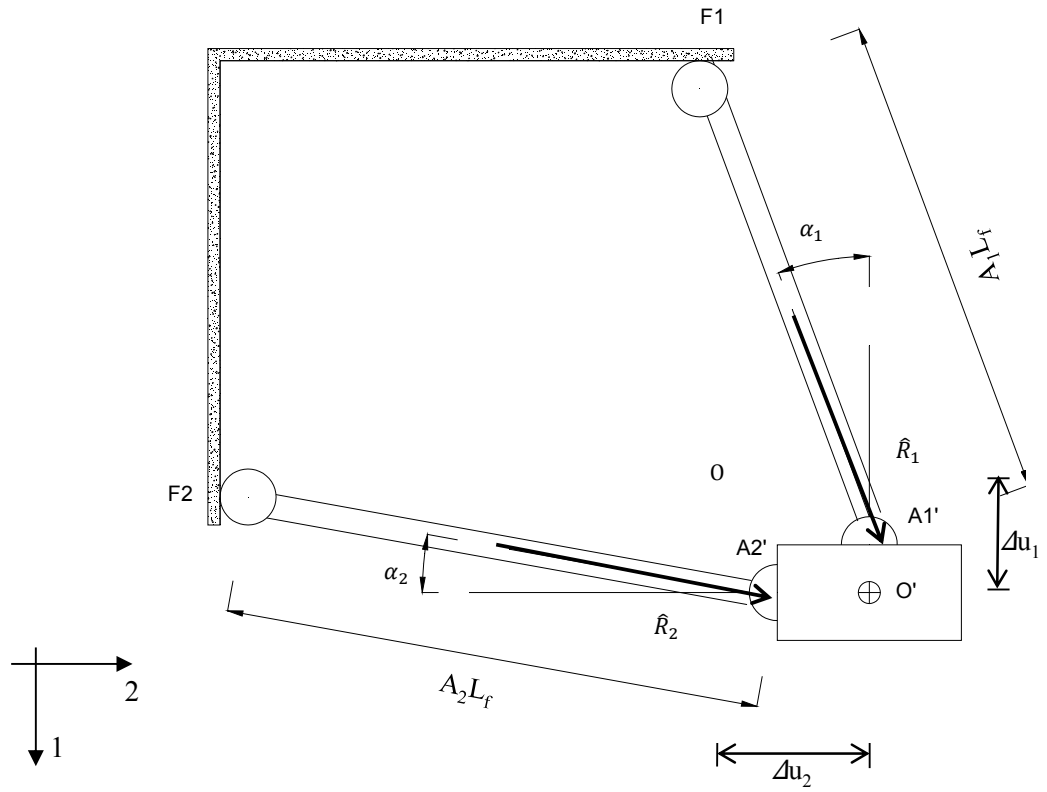

Figure 3-3 A typical displaced position

Consider now a typical displaced position shown in Figure 3-3, where

A_1L_f : current length of Actuator 1
A_2L_f : current length of Actuator 2
O' : current position of the column geometric centre
α_1 : the acute angle between the current direction of Actuator 1 and the *1* axis
α_2 : the acute angle between the current direction of Actuator 2 and the *2* axis
Δu_1 : change in displacement in the *1* direction
Δu_2 : change in displacement in the *2* direction
$\hat{R}_1$: restoring force in the directions of Actuator 1 orientation
$\hat{R}_2$: restoring force in the directions of Actuator 2 orientation
A1', F1 : current position of end nodes of Actuator 1
A2', F2 : current position of end nodes of Actuator 2

In this configuration, A_1L_f and A_2L_f can be deduced directly from the measurements taken by the internal displacement transducers inside each actuator, that is

$$A_kL_f = A_kL_0 + T_k^d$$

where *k* identifies the actuator (1 or 2), and T_k^d represents the linear displacement measured by the internal displacement transducer of Actuator *k*. Once are A_1L_f and A_2L_f obtained, they can be used as input to solve for Δu_1 and Δu_2. This then provides a means to establish and control the new location of the column (*O'*). The algorithm assumes the following,

- the column is rigid in plane. i.e, any point on the column faces is displaced by the same amount in the plane of the column cross-section;
- the column displacements are in-plane only. i.e. Vertical displacement due to the rocking motion is neglected.

The non-linear geometric constraint equations can be written as,

$$F_1 : 0 = (A_1L_0 + \Delta u_1)^2 + (\Delta u_2)^2 - (A_1L_f)^2$$

$$F_2 : 0 = (A_2L_0 + \Delta u_2)^2 + (\Delta u_1)^2 - (A_2L_f)^2$$

An iterative Newton-Raphson procedure is then used to solve for $\Delta u_1$and Δu_2. This is defined by the following general expression,

$$[X]_{n+1} = [X]_n - [J[X]_n]^{-1}[F[X]_n]$$

where *J* is a Jacobian matrix for *[F]*. For this specific algorithm, *J* is defined as

$$J = \begin{pmatrix} \frac{\partial F_1}{\partial \Delta u_1} & \frac{\partial F_1}{\partial \Delta u_2} \\ \frac{\partial F_2}{\partial \Delta u_1} & \frac{\partial F_2}{\partial \Delta u_2} \end{pmatrix} = 2\begin{pmatrix} A_1L_0 + \Delta u_1 & \Delta u_2 \\ \Delta u_1 & A_2L_0 + \Delta u_2 \end{pmatrix}$$

The iteration process is then terminated once convergence is achieved within some predetermined tolerance.

Once Δu_1 and Δu_2 has converged, the orientation of each actuator relative to its original orientation can be calculated as

$$\alpha_1 = \tan^{-1}\left(\frac{\Delta u_2}{A_1L_0 + \Delta u_1}\right)$$

$$\alpha_2 = \tan^{-1}\left(\frac{\Delta u_1}{A_2L_0 + \Delta u_2}\right)$$

The load cell in each actuator measures the restoring force from the column in the current direction of each actuator $\hat{R}_1$ and $\hat{R}_2$. Consequently, they must be transformed back into forces in the original coordinate system, R_1 and R_2. This can be achieved by the following transformation matrix,

$$\begin{pmatrix} R_1 \\ R_2 \end{pmatrix} = \begin{pmatrix} \cos\alpha_1 & \sin\alpha_2 \\ \sin\alpha_1 & \cos\alpha_2 \end{pmatrix} \begin{pmatrix} \hat{R}_1 \\ \hat{R}_2 \end{pmatrix}$$

These nodal displacements $\Delta u_1$and Δu_2, and restoring forces R_1 and R_2, provide the feedback variables for the PSD algorithm to determine the target displacements u_1 and u_2 for the next step. Since these target displacements are in the original coordinate system, they must be transformed to account for the current orientation of actuators. The target displacements at the current orientations of the actuators, $u_{1,A}$ and $u_{2,A}$ are derived according to the following relationship

$$u_{k,A} = \frac{1}{\cos\alpha_k}(u_k + A_k L_0(1-\cos\alpha_k))$$

where

$A_k L_0$: initial length of Actuator *k* (1 or 2)
$u_{k,A}$: target displacement in the direction of Actuator *k* (1 or 2)
u_k : target displacement in the direction DOF *k* (*1*- or *2*- axis)
α_k : last orientation of actuator *k* ($\alpha_1$or α_2)

The process is repeated each time new target displacements are required.

4.0 Methodology

The experimental programme is divided into two parts,

A. Series of bi-directional PSD tests following three different loading strategies for each loading substep, and
B. Series of pseudostatic cyclic pushover tests following four different loading patterns.

The loading strategies for test series A are as shown in Figure 2-1. Loading strategy III in the figure denotes the most direct load path where the specimen is displaced in both principal directions simultaneously. While, loading strategies I and II denote the other extremes where the column is displaced in each principal direction at a time. This series of test evaluates the effect of load paths on the results from PSD tests.

The four loading patterns for test series B are as shown in Figure 4-1. These patterns were developed based on ACI guidelines [10]. These tests applied rounds of increasing displacements following the different paths. The four paths considered were,

- Linear – where cyclic displacements are increased and decreased in both principal axes simultaneously.
- Circular – where cyclic displacements follow a circular pattern in plan, and the rates of displacement application are increasing and decreasing in the two principal directions.
- Diamond – where cyclic displacements follow a diamond pattern in plan, and the rates of displacement applications are constant but increasing and decreasing respectively in the two directions.
- Clover – Where cyclic displacements follow a clover leaf pattern in plan.

These tests directly consider the effect of loading history and loading paths on commonly used laboratory test results.

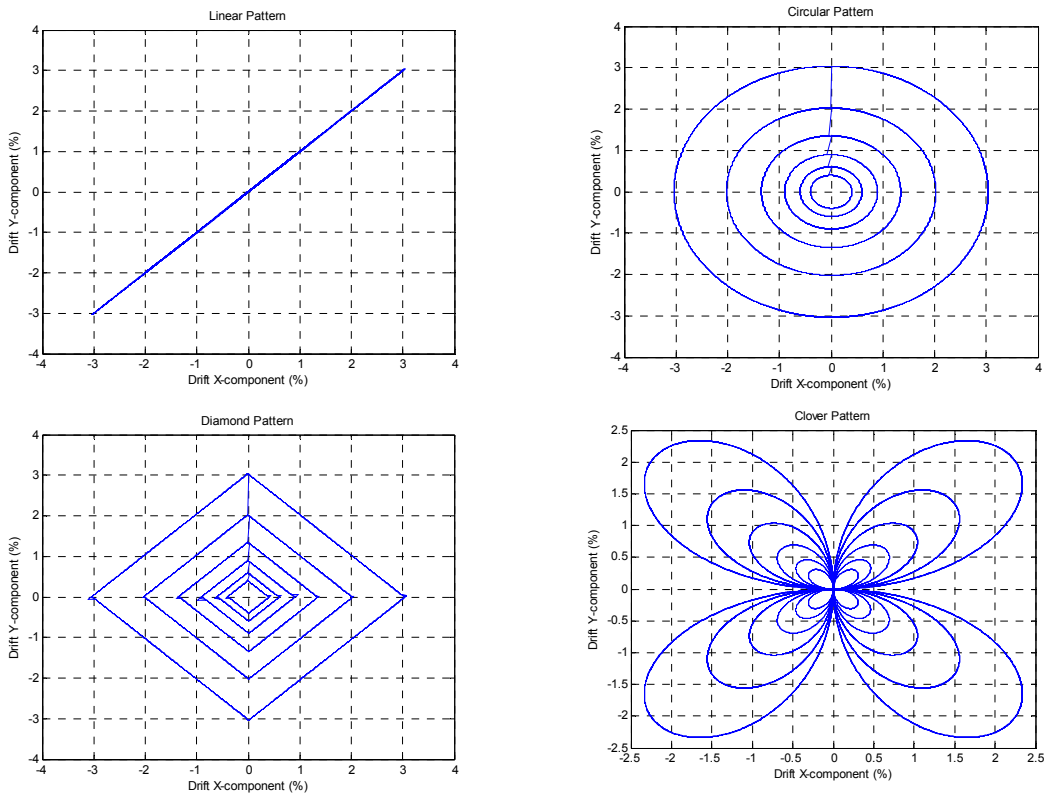

Figure 4-1 Displacement patterns for the pseudostatic experiment

4.1 Testing Matrix

Six sets of earthquake ground motion were considered for the PSD tests in test series A. For each set of ground motion, the tests were repeated for the three different loading strategies. The earthquake records were selected and scaled based on the NZS1170.5:2005 [11]. Figure 4-2 shows the site-specific target acceleration spectrum and the response spectra of the individual scaled earthquake records. The earthquake records were scaled to fit the target spectrum for the period range of $0.4s$ to $1.3T_1$, where $T_1$was the largest translational period in the direction of interest, i.e. the effective period T_e.

The pseudostatic tests in test series B applied six sets of cyclic deformations to the column for each of the four different loading patterns. The sets of cyclic deformations were increasing in amplitudes and were measured as multiples of the yield displacement, also known as the ductility factor (μ). Three cycles of loading were applied at each of the ductility levels μ = ⅔, 1, 1.5, 2.25, 3.5 and 5. Except for the linear pattern, where the rate of the load imposed was constant throughout the test, the rate of loading during the pseudostatic tests varied. The actuators were limited to a maximum loading rate of 1.5 mm/s for all tests in test series B. Table 4-1 summaries the different experiments for this study.

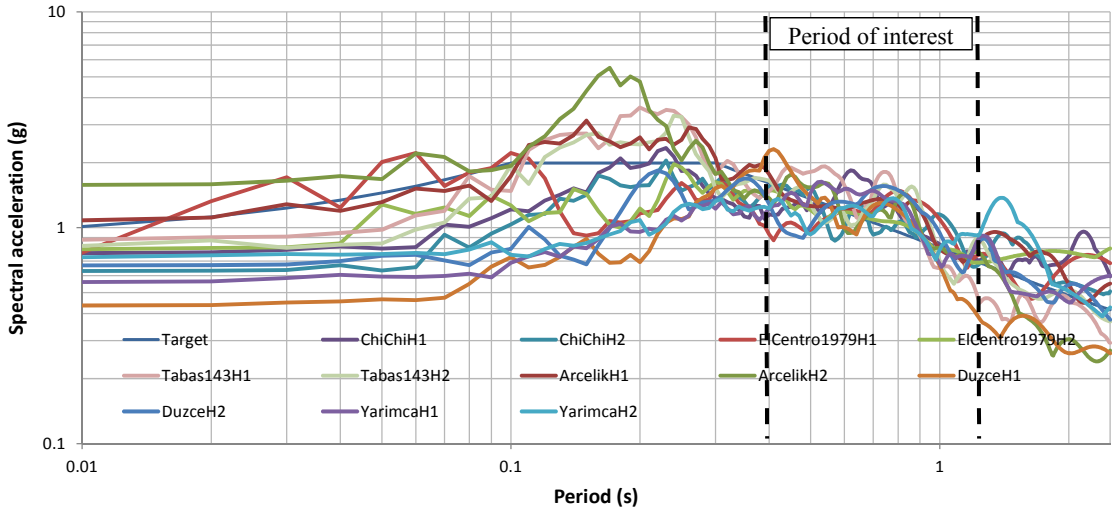

Figure 4-2 Spectral accelerations of the scaled earthquake records used in the testing regime

Loading pattern	Description	Displacement Pattern			
PSD EQ A	Biaxial pseudodynamic test Scaled 1987 Tabas 143, Iran	Pattern I	Pattern II	Pattern III	
PSD EQ B	Biaxial pseudodynamic test Scaled 1999 Duzce, Turkey	Pattern I	Pattern II	Pattern III	
PSD EQ C	Biaxial pseudodynamic test Scaled 1999 Chi-Chi, Taiwan	Pattern I	Pattern II	Pattern III	
PSD EQ D	Biaxial pseudodynamic test Scaled 1999 Arcelik, Turkey	Pattern I	Pattern II	Pattern III	
PSD EQ E	Biaxial pseudodynamic test Scaled 1940 ElCentro	Pattern I	Pattern II	Pattern III	
PSD EQ F	Biaxial pseudodynamic test Scaled 1999 Yarimca, Turkey	Pattern I	Pattern II	Pattern III	
QS	Biaxial quasi-static test	Linear	Diamond	Circular	Clover

Table 4-1 Experiment matrix

4.2 Prototype Structure and the Test Specimen

The specimen used in the experiments was an unbonded post-tensioned (PT) reinforced concrete (RC) column with asymmetrical cross-section. The column was designed to rock elastically under lateral loading. Furthermore, replaceable mild-steel bars were mounted externally to provide additional energy dissipations and to recreate a plastic response. A rocking column was selected as the test specimen to ensure the specimen do not degrade and tests can be reliably repeated and thus removing a source of discrepancies between trials. A rocking mechanism prevents the formation of plastic hinge and damage that usually occurs at the base of a monolithic column. The unbonded PT bars improve the stability of the rocking column, preventing it from toppling and gives rise to a stable positive post-uplift stiffness. The overall behaviour is essentially non-linear elastic with small amount of energy dissipation from the externally mounted energy dissipators (EMD). The system is expected to produce a "flag-shaped" hysteretic curve typical for rocking structures [12].

The column specimen was sized to represent a 1:3 scale prototype bridge pier and envisaged to be a part of a large span bridge system, such as that shown in Figure 4-3. The bridge pier was designed using Direct Displacement Based Design (DDBD) procedure [13]. The DDBD procedure uses an equivalent single degree of freedom (SDOF) substitute structure with secant stiffness to the target displacement at Maximum Considered Earthquake. Table 4-2 summarizes the parameters defining the elastic hazard spectrum according to [11] for the column being tested. This design followed closely to the column tested by Marriot [14].

Table 4-3 presents a summary of the model and prototype column dimensions in the experiment, and Figure 4-4 presents a schematic of the laboratory setup. The model column, herein referred to as the column, was detailed with 12 – D10 (10mm diameter, Grade 300 MPa, deformed bar) as longitudinal reinforcements, and three D10 rectangular hoops at 120 mm centres as transverse reinforcements. A 30x30x3 steel equal angle was cast into the concrete around the column base perimeter to minimise damage due to rocking impacts. Horizontal ducts were also cast into column base for attaching the steel brackets to hold the replaceable externally mounted mild steel bars (energy dissipators). Due to reinforcement congestions, chemical anchors were used to mount the steel brackets on the shorter column face. Concrete with 40 MPa unconfined compressive strength was use for the column and the column foundation. Concrete cylinder tests completed on the day of testing confirmed the concrete quality.

The concrete column sits in the opening of a perimeter steel base plate. This base plate prevents sliding of the column upon rocking and provides anchorage of the EMDs.

A selection of photographs taken during construction are shown in Figure 4-5 and engineering drawings of the column, foundation and steel brackets are provided in Appendix A.

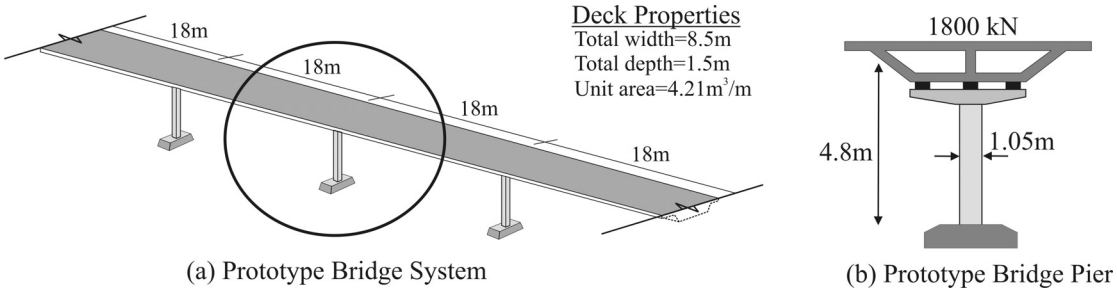

(a) Prototype Bridge System (b) Prototype Bridge Pier

Figure 4-3 Prototype bridge system

Structural design parameters according to NZS 1170.5	
Soil Site class	Site class C
$\boldsymbol{Z}$	0.4
$\boldsymbol{T_R}$	2000 years
$\boldsymbol{R}$	1.7
$\boldsymbol{D}$	8 km
$\boldsymbol{N_{(T_1,D)}}$	Varies depending on the fundamental period [11]
$\boldsymbol{S_P}$	1.0
$\boldsymbol{C(T_1 = 0) = PGA}$	0.301

Table 4-2 Seismic hazard parameters

	Prototype	Model
Cross-section area	1.1025 m^2	1.225×10^5 mm^2
Cross-section dimension	$1.05 \times 1.05\ m$	$490 \times 250\ mm$
Pier height	$4.8\ m$	$1.6\ m$
Participating deck gravity load	$900\ kN$	$100\ kN$

Table 4-3 Properties of prototype and model of bridge pier

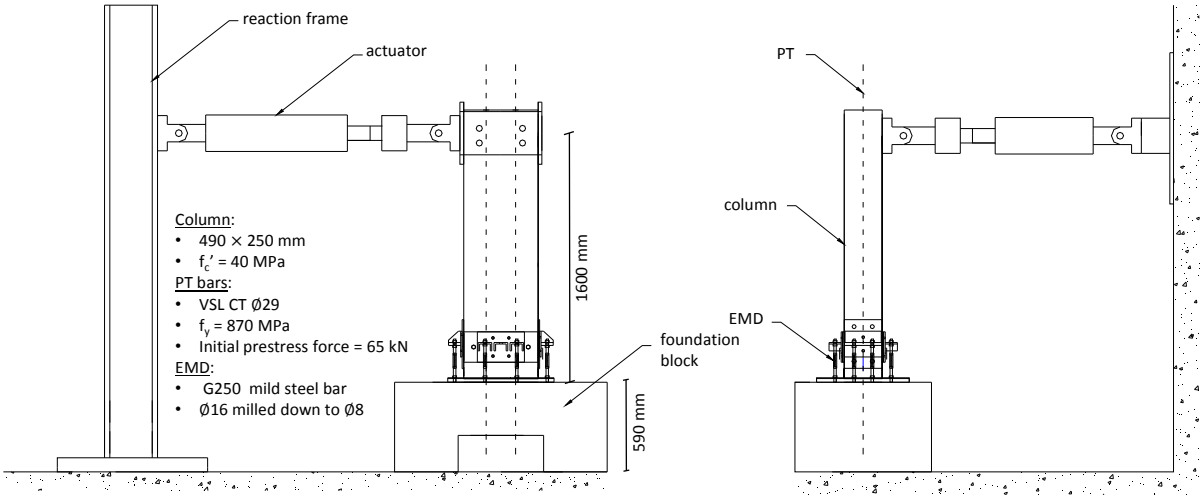

Figure 4-4 Elevation view of test setup, stronger axis face (left) and weaker axis face (right)

(a) Vertical ducts for PT bars

(b) Cast in place steel equal angle welded to main reinforcements

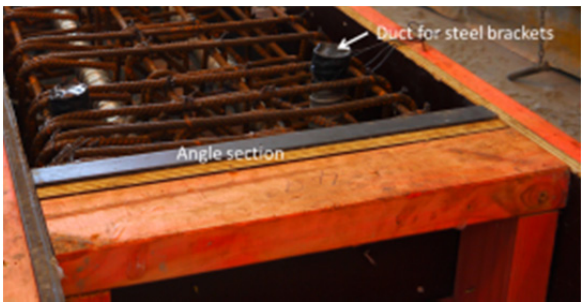

(c) Duct at column base for attaching steel bracket to column face

(d) Freshly casted column

Figure 4-5 Photographs showing the construction sequence of the unbonded PT column

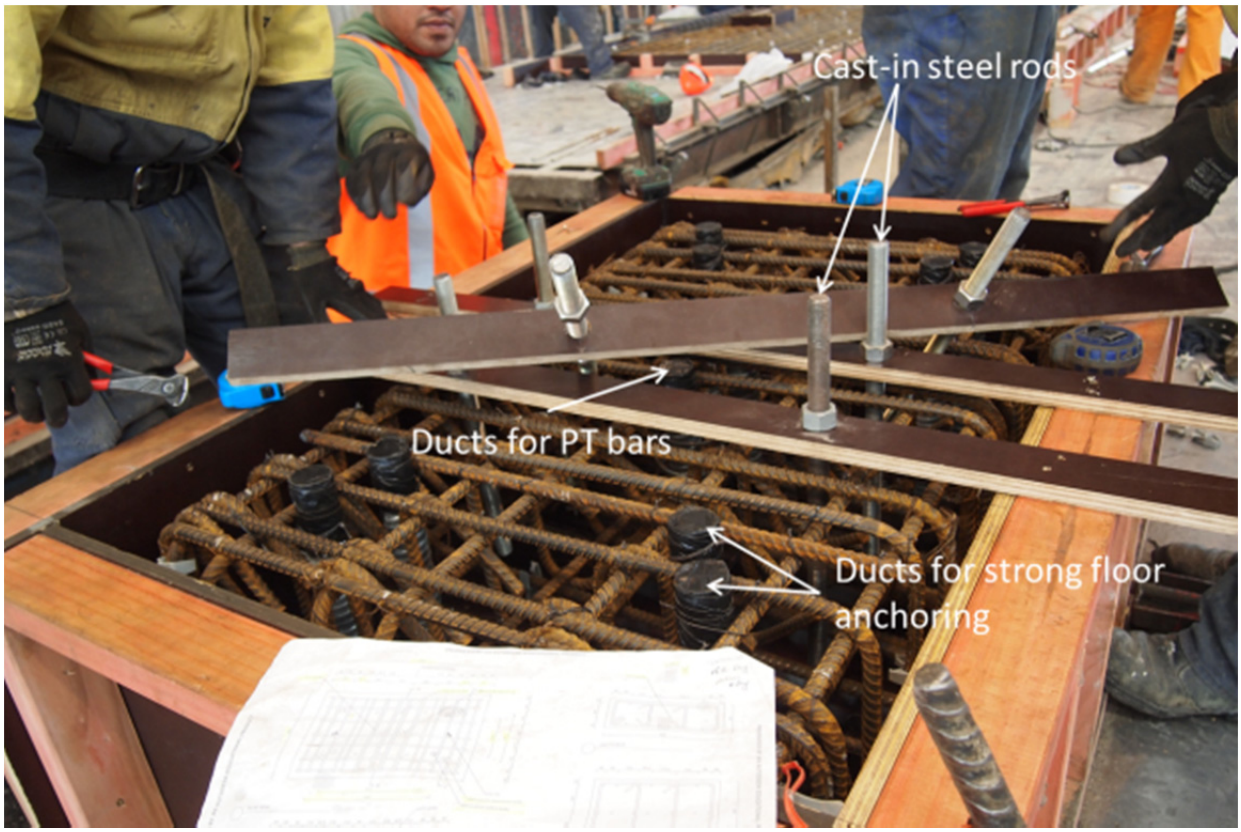

(a) Reinforcement arrangement of the concrete foundation block. Ducts were inserted for tensioning of the PT bars and securing the foundation block to the laboratory strong floor. Cast-in steel rods provided anchorage to the steel base plate

(b) Casting of concrete into foundation block

(c) View of the cast-in steel bolt head after pouring

Figure 4-6 Photographs showing the column foundation construction sequence

5.0 Results

This report presents a selection of the results from the pseudostatic and PSD tests. The results highlight the importance of conducting multi-axial testing in the laboratory and also demonstrate the functional status of the biaxial PSD testing facility at the University of Auckland.

5.1 Pseudostatic Test (Test Series A) Results

Figure 5-1 presents individually the force displacement response of the column from the pseudostatic cyclic tests for each loading pattern, shown separately for each axis of loading. In these figures, X direction displacements are parallel to the larger dimension of the column cross-section and represent major axis bending.

The force-deformation curves exhibited the expected flag-shaped behaviour of a self-centering system with hysteretic energy dissipators. The results showed that different loading patterns produced distinctly different strength and energy dissipation characteristics.

It can be observed from Figure 5-1 that only the linear displacement pattern produced similar energy dissipation in the positive and negative directions for both axes of loading. The other patterns dissipated more energy in one direction than the other. This can be explained by the fact that the specimen was essentially loaded about a single bending axis under the linear displacement pattern, while the resultant bending axis is constantly changing in the other loading patterns. Coupled this with greater EMD extension due to the different load paths, extra bending actions and consequently misaligned compressive load on return cycles, it led to greater opportunities for disspator buckling and hence plastic deformations in the non-linear displacement patterns, similar in concept as a “ratcheting” phenomenon.

Table 5-1 details the amount of energy dissipation in the different tests, in the different directions expressed as equivalent viscous damping.

Figure 5-2 presents the strength envelopes developed from the pseudostatic tests. The figure shows that displacement paths have a significant effect on the final strength definition. The diamond displacement pattern produced the highest early strength and highest initial stiffness. This was followed by the clover displacement pattern and then the linear displacement pattern when each direction was considered in isolation. This can be explained by considering the out-of-plane displacement during an increasing in-plane displacement cycle.

Consider the case when X direction displacement is increased from zero to a peak value using the diamond displacement pattern, the corresponding Y displacement would decrease from the peak value to zero. For a post-tensioned rocking specimen, the initial Y displacement would have caused considerable uplift and hence large axial force in the PT bars and large restoring strength even at very low X displacement. Conversely, under the linear displacement pattern, both X and Y direction displacements grow from zero to the peak value simultaneously and there is less axial force in the PT bar initially and hence it produces a lower strength value for a given X displacement. Figure 5-3 shows the variation of PT force as a function of X and Y direction displacements under the different displacement pattern.

This highlights the importance of considering multi-axial displacements when establishing a system’s basic force-displacement relationship, and when conducting physical experiments.

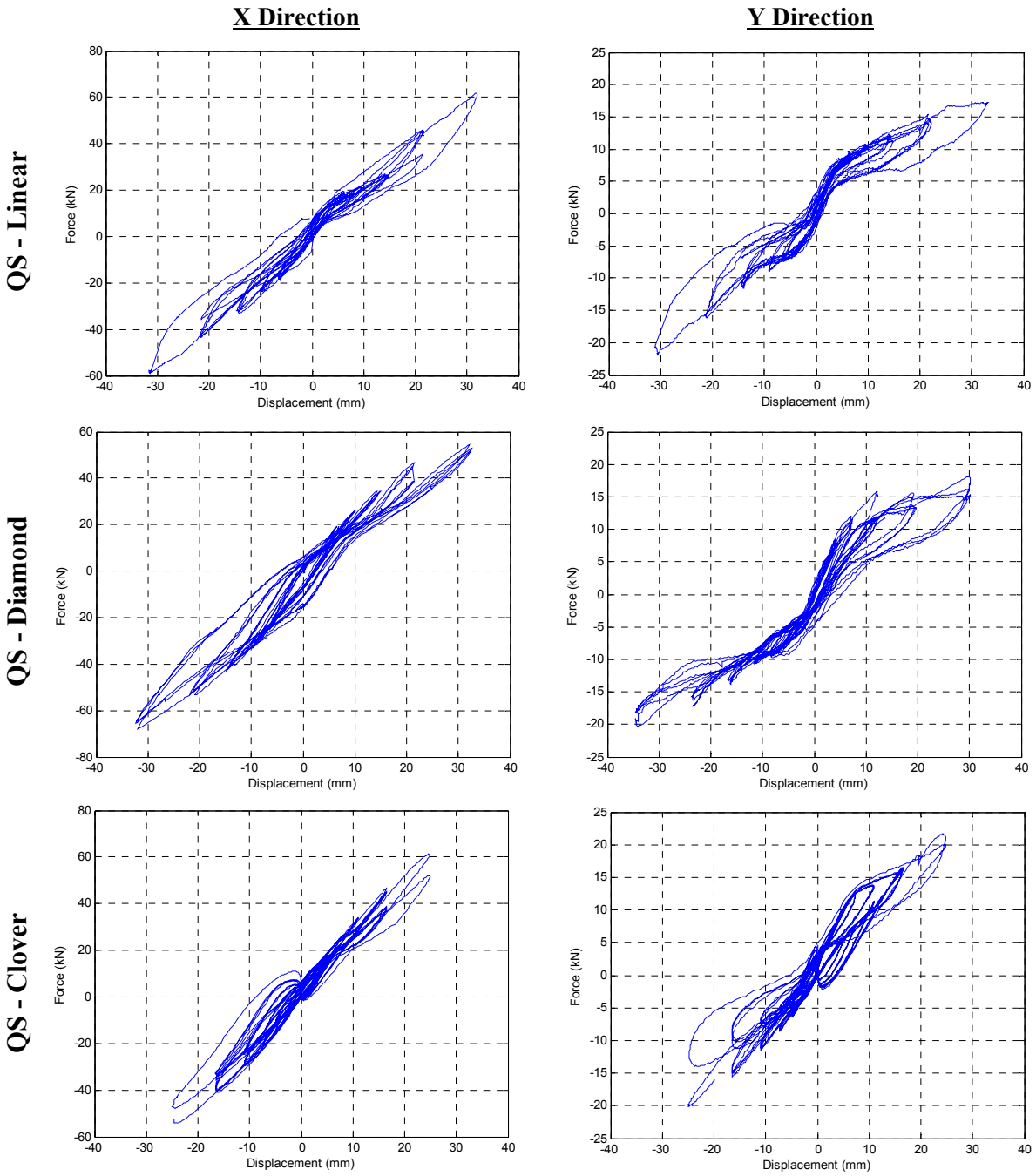

Figure 5-1 Pseudostatic force-displacement response of the column under different loading patterns
(Note. QS - Circular pattern results have not been analysed)

	Equivalent viscous damping (ξ) %						
	X direction			Y direction			Combined
	+ ve	- ve	Average	+ ve	- ve	Average	
QS - Linear	6.0	9.0	7.7	3.0	3.6	3.3	11.0
QS - Diamond	1.5	3.3	2.2	3.3	1.1	2.7	7.4
QS - Clover	6.2	6.8	6.5	4.4	3.8	4.2	12.0

Table 5-1 Equivalent viscous damping based on pseudostatic tests under different loading patterns

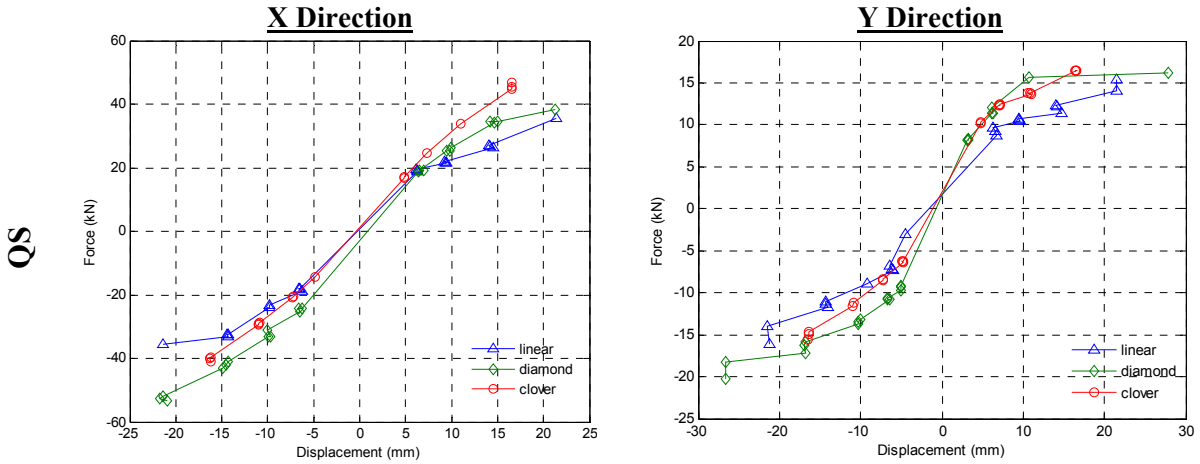

Figure 5-2 Pseudostatic force-displacement envelope of the column under different loading patterns

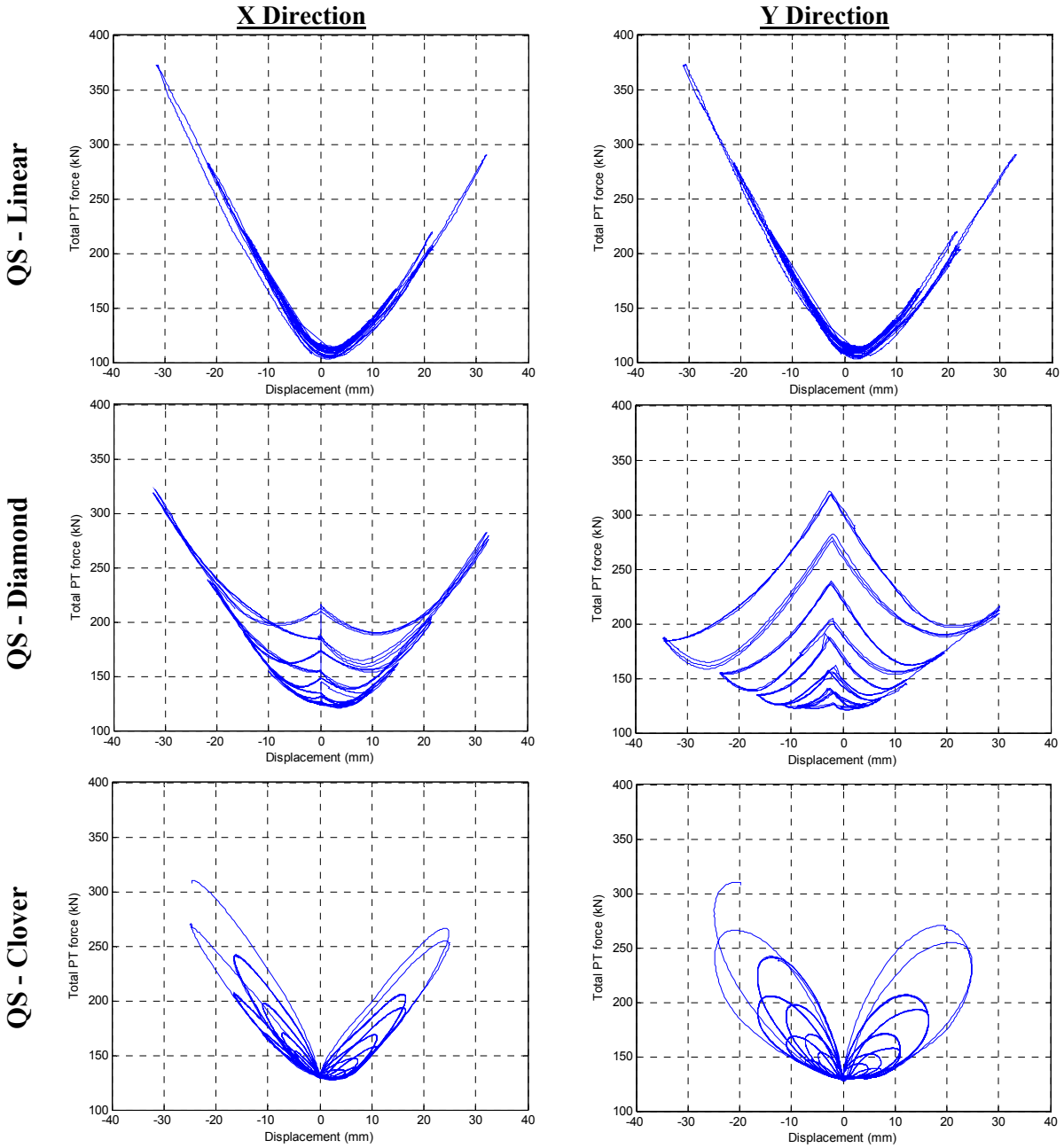

Figure 5-3 PT force-displacement history under different loading patterns

5.2 PSD Test (Test Series B) Results

Test series B comprised of six sets of PSD tests. For brevity, only three sets of the tests will be covered in this report, namely PSD EQ A (Tabas), PSD EQ B (Duzce) and PSD EQ F (Yarimca). For these tests, the specimen represented a prototype bridge pier and it was subjected to bidirectional earthquake ground motion input via the PSD method. Unlike test series A, the displacement histories for the structure were not known prior to the tests, but they were interactively determined from the underlying numerical model during testing. Within each set of the PSD tests, the tests were repeated following three different displacement tracking strategies, as shown in Figure 2-1, when applying each sub-load step.

The column displacement time histories and force displacement response during the three earthquake simulations are shown in Figure 5-4 to Figure 5-9.

These figures highlight differences in amplitude and phase of the column displacements in both axes due to the different displacement tracking strategies. This is most clearly shown by the very different displacement trace in plan view shown in Figure 5-5, Figure 5-7, and Figure 5-9. It should be noted that a classical flag-shaped hysteretic curves did not develop, and that appreciable residual drifts were present. This was in part caused by a large crack at one corner of the column and therefore sliding, opening and closing of this crack dominated the hysteretic behaviour. The figures also highlighted poor performance of the EMD due to buckling and slippage.

In the absence of true reference result from full dynamic tests (e.g. shake-table test), or idealised numerical simulation, the tracking strategy Path III can be thought as the ideal solution considering the shortest path is the most plausible. For each tracking strategy, the amplitudes attained at every half-cycle in the displacement time history are identified. Figure 5-10 shows an example of the identified amplitudes, positives and negatives from PSD EQ B (Duzce). The amplitudes attained by tracking strategies Path I and Path II can then be quantified in term of their differences, or errors, relative to Path III. Mathematically, these amplitude differences can be represented as a normalised error ε defined as,

$$\varepsilon_i = \frac{A^i - A^{III}}{A^{III}}$$

where A = displacement amplitude and i = I or II e.g. A^i indicates displacement amplitudes attained during Path i test. Consequently any negative values ε indicate that the attained amplitudes in Path I or II are smaller than the reference value Path III, while positive values indicate the opposite.

Collating the normalised amplitude errors from each cycle in the earthquake time histories, Figure 5-11 plots the distributions of these errors as a density function, $f_X(x)$. In each plot, a solid black line parallel with the vertical axis is drawn at zero ε. If different displacement paths, on average, produced the same amplitudes displacement, this would be indicated by the peak (median) of the density function coinciding with this line.

It is interesting to note that the median values of ε across all results are mostly positive, i.e. the amplitudes at peaks of each cycle attained via Path I and II are generally larger than Path III. During Path I or Path II tests, the column displaced a greater distance compared to Path III, providing greater opportunity for increased plastic deformation in the column. Therefore it is likely that the column developed a lower restoring force which in turn led to larger displacement in the PSD algorithm.

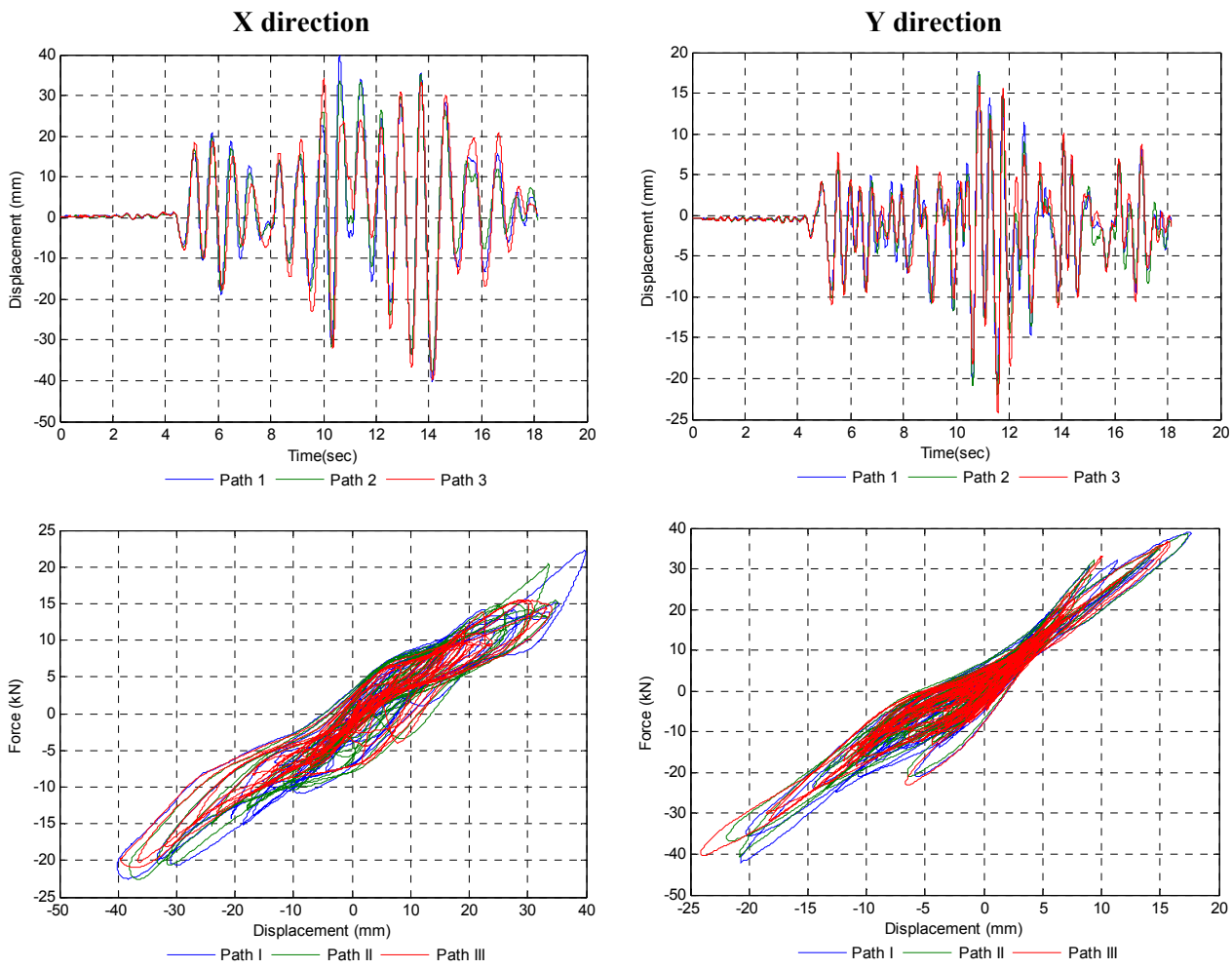

Figure 5-4 Displacement time history and force-displacement response from PSD EQ A (Tabas) test

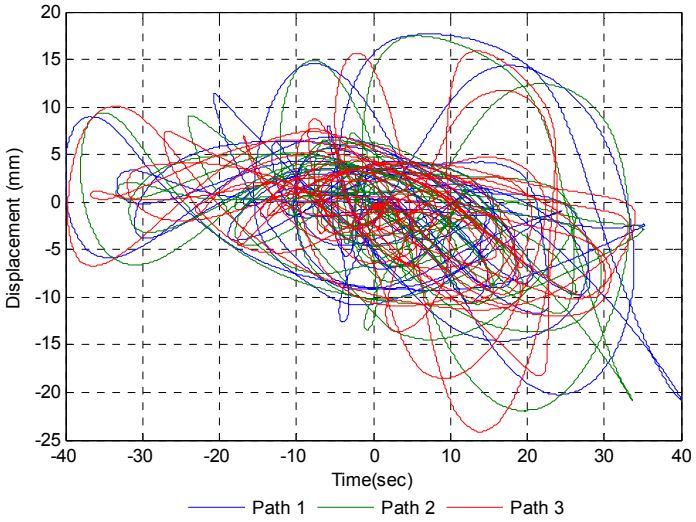

Figure 5-5 Top of column displacement during PSD EQ A (Tabas) viewed in plan

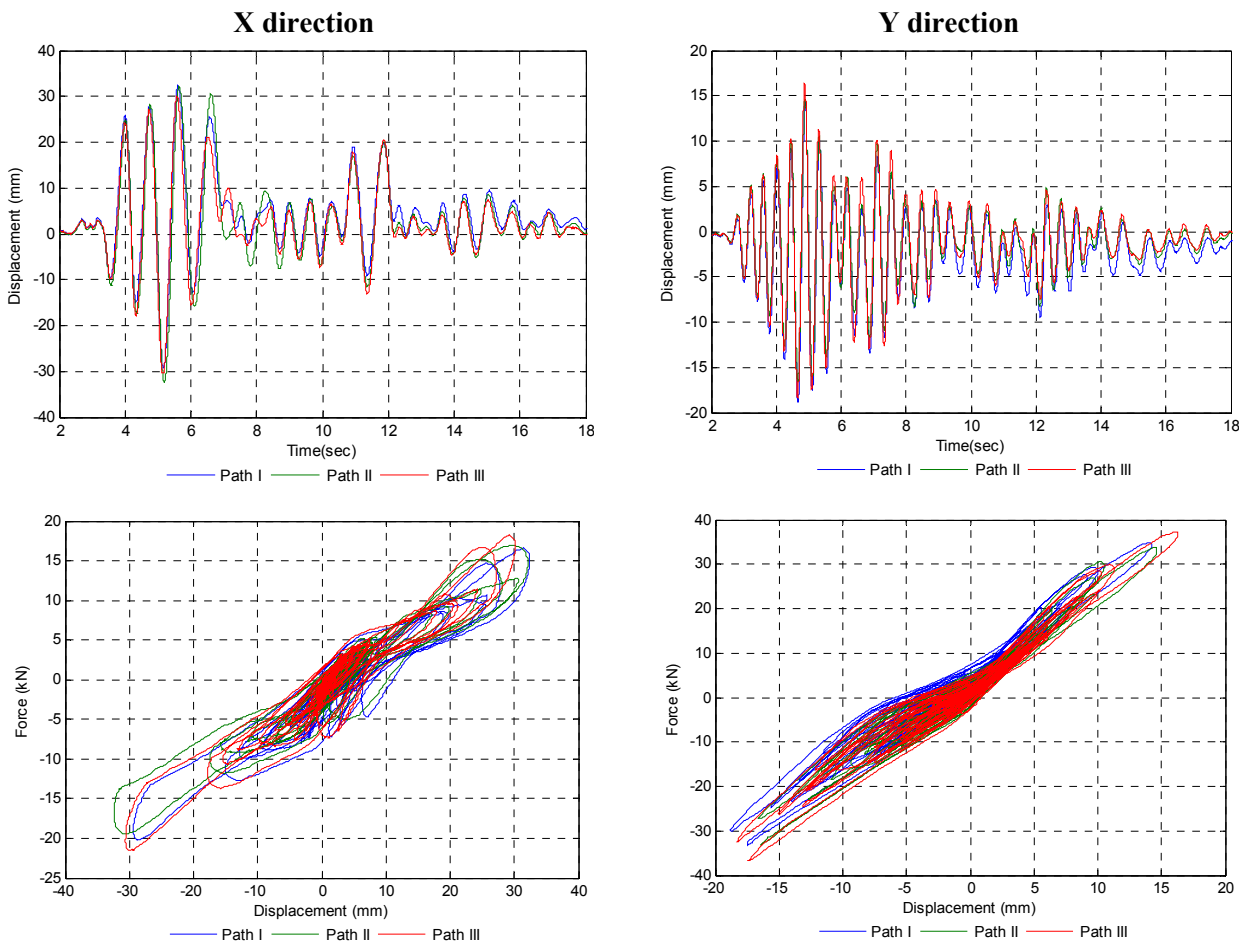

Figure 5-6 Displacement time history and force-displacement response from PSD EQ B (Duzce) test

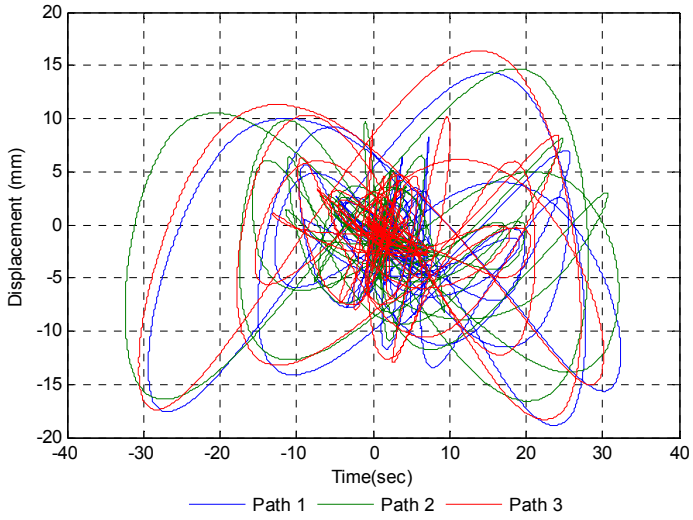

Figure 5-7 Top of column displacement during PSD EQ B (Duzce) viewed in plan

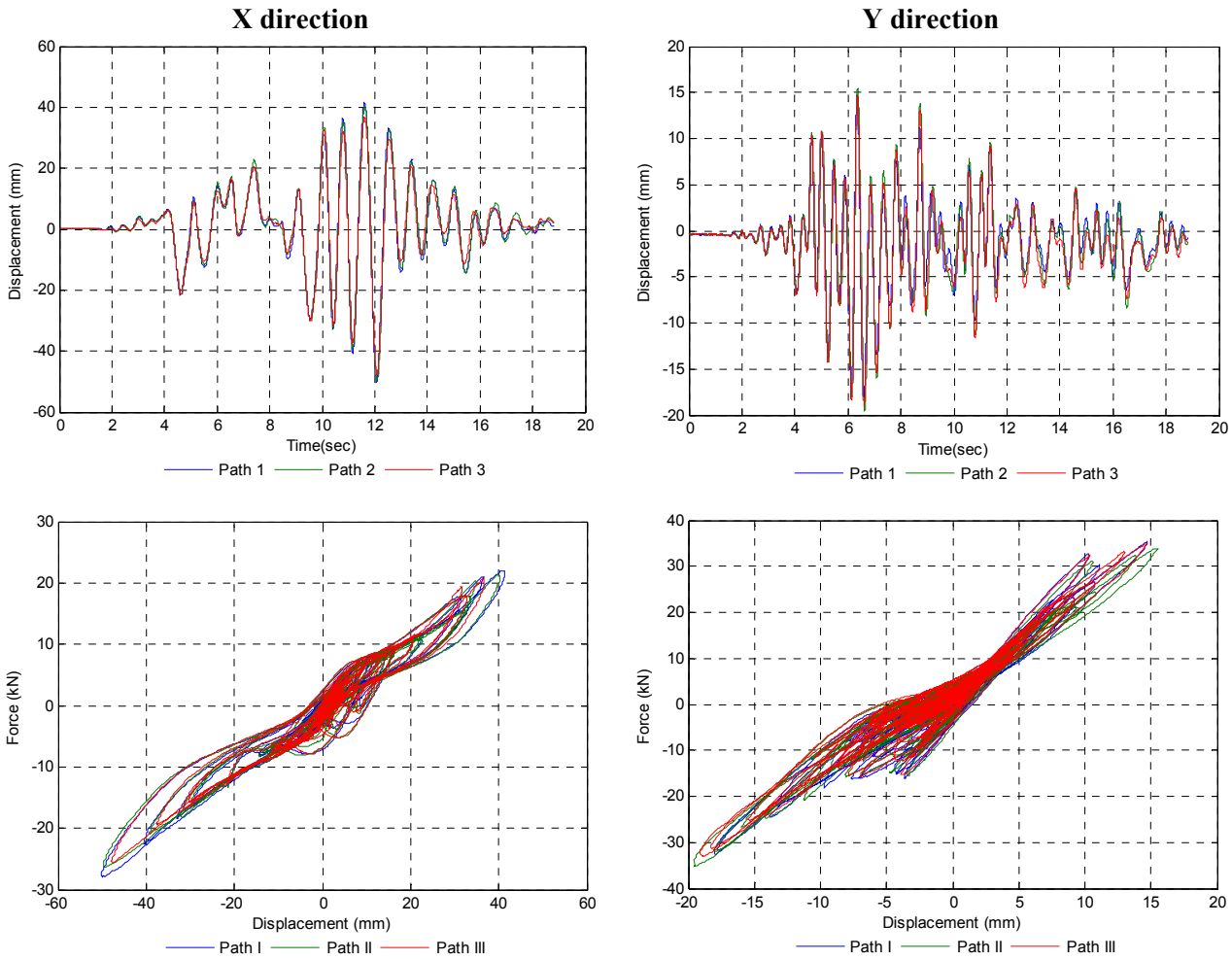

Figure 5-8 Displacement time history and force-displacement response from 1999 Yarimca earthquake

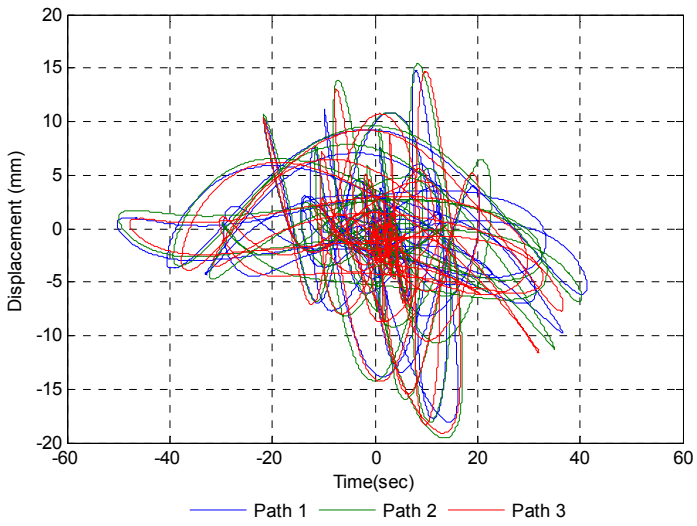

Figure 5-9 Top of column displacement during PSD EQ F (Yarimca) viewed in plan

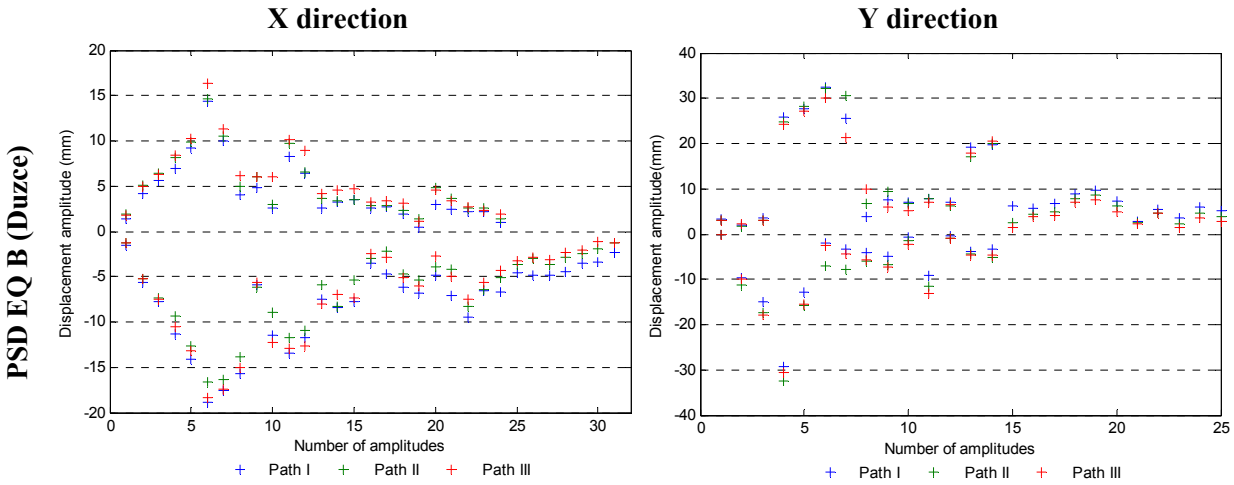

Figure 5-10 Peak displacement amplitudes during PSD EQ B (Duzce) simulation

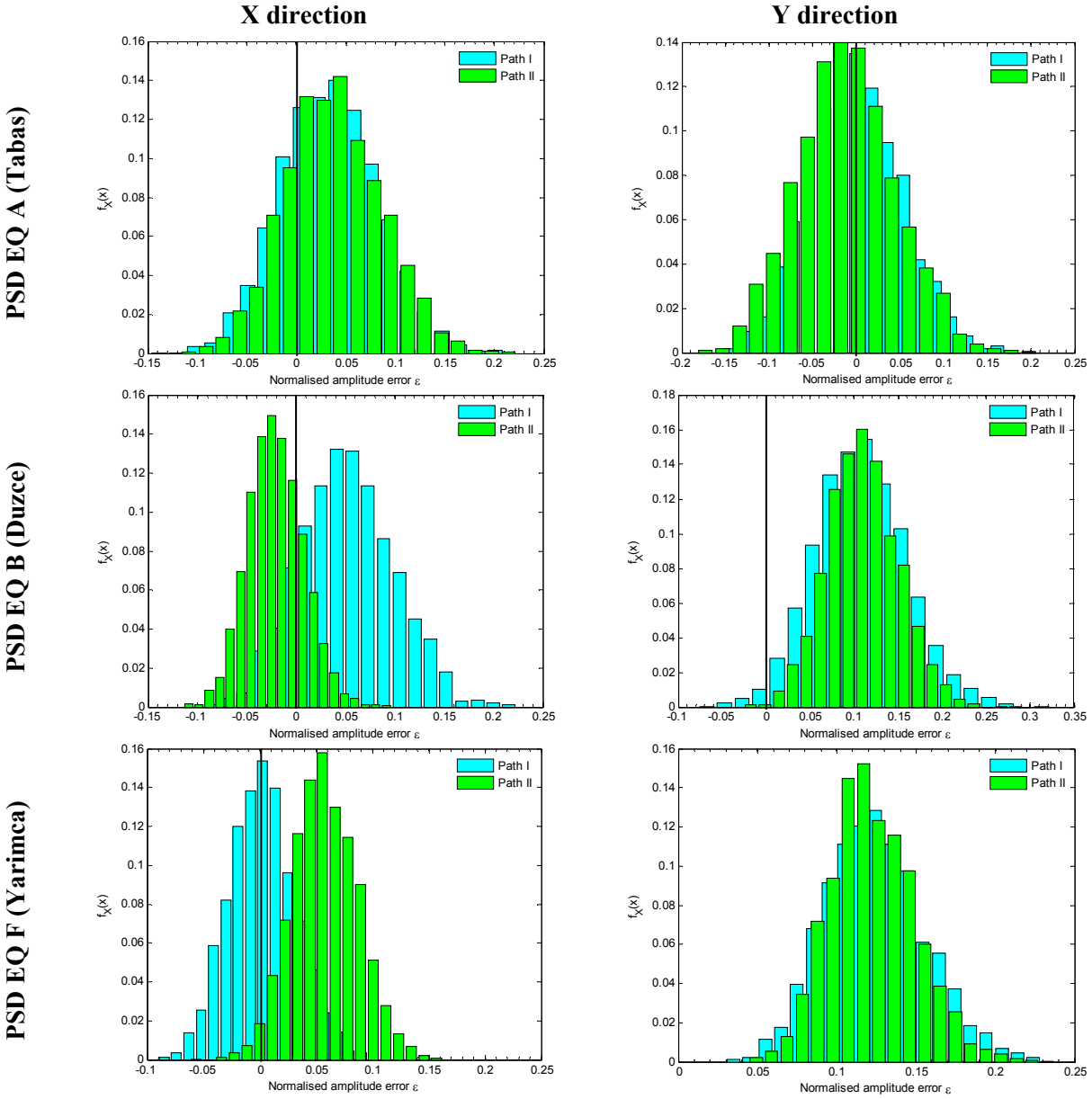

Figure 5-11 Distribution of normalised amplitude errors from the PSD simulations

6.0 Conclusion

This report presents the results of a major experimental project evaluating the pseudostatic and dynamic response of a rocking column with replaceable externally mounted energy dissipators. The project subjected the column to bidirectional cyclic pseudostatic pushover using four displacement patterns, and a series of simulated earthquake excitations using PSD testing technique with three displacement tracking strategies. This amounted to a total of 22 tests, including 4 pseudostatic tests and 18 PSD tests. The tests were conducted on the same rocking column specimen as it was specifically designed as a low damage element. The experiments investigated the effects of displacement paths and loading sequences had on the response of inelastic structures and accuracies of biaxial PSD tests.

The pseudostatic tests showed that different loading patterns produced distinctly different strength and energy dissipation characteristics. The exact two dimensional loading path was found to be an important factor as it altered the axial load on the rocking column and hence the strength envelope. Furthermore, different displacement loading paths led to different principal bending axis which for the non-linear loading patterns had demonstrated to promote ratcheting.

The PSD tests showed that different displacement tracking strategies or more generally displacement paths affect the amplitude and phase of PSD test results. This in turns are further subjected to history dependent errors. A statistical analysis of the results highlighted that deviation from the most direct loading path tends to produce greater displacements due to increased plastic deformation in the column and lower restoring force.

Publications from this project

- Gultom, R., and Q. T. Ma. “Biaxial pseudodynamic tests of a post-tensioned rocking column with externally mounted energy dissipators.” *Proceedings of the New Zealand Society for Earthquake Engineering Annual Conference, Rotorua, New Zealand 2015*
- R. Gultom, and Q. T. Ma. “Intuitive Real-Time Compensation Algorithm for Actuator Control Errors in Fast Pseudodynamic Tests.” *Bulletin of the New Zealand Society for Earthquake Engineering,* **47** (1), 15-27, 2014.
- R. Gultom, and Q. T. Ma. “Intuitive Real-Time Compensation Algorithm for Actuator Control Errors in Fast PSD Tests.” *Tenth US National Conference on Earthquake Engineering*: Frontiers of Earthquake Engineering, Anchorage, Alaska, USA. July 21-25 2014
- R. Gultom, and Q. T. Ma. “Accuracy of biaxial pseudodynamic tests on a rocking post-tensioned column subject to displacement tracking strategies” Journal of Strucutral Engineering (In preparation)

Acknowledgement

The authors wish to thank the Earthquake Commission for the financial support of this project through the Biennial Research Funding Programme, project BIE12/632.

References

[1] M.P. Collins, D. Mitchell, P. Adebar, F.J. Vecchio. A general shear design method. *ACI Structural Journal,* **93** (1), 1996.

[2] K. Takanashi, K. Udagawa, M. Seki, T. Okada, H. Tanaka. Nonlinear earthquake response analysis of structures by a computer-actuator on-line system. *Bulletin of Earthquake Resistant Structure Research Center,* **8**, 1-17, 1975.

[3] S.A. Mahin, P.B. Shing. Pseudodynamic method for seismic testing. *Journal of Structural Engineering,* **111** (7), 1482-503, 1985.

[4] G. Magonette. Development and application of large–scale continuous pseudodynamic testing techniques. *Philosophical Transactions of the Royal Society of London. Series A: Mathematical, Physical and Engineering Sciences,* **359** (1786), 1771-99, 2001.

[5] X. Chen, S. Yan, B. Ji. Pseudo-dynamic test and numerical simulation of high-strength concrete frame structure reinforced with high-strength rebars. *Earthquake Engineering and Engineering Vibration,* **10** (2), 303-11, 2011.

[6] S.-Y. Chang. Bidirectional Pseudodynamic Testing. *Journal of Engineering Mechanics,* **135** (11), 1227-36, 2009.

[7] J. O'Hagan, Q. T. Ma, Effects of actuator tuning on pseudo-dynamic tests. Paper presented at the Ninth Pacific Conference on Earthquake Engineering Auckland, New Zealand, 14-16 April 2011.

[8] R. Gultom, Q. T. Ma. Intuitive Real-Time Compensation Algorithm for Actuator Control Errors in Fast Pseudodynamic Tests. *Bulletin of the New Zealand National Society for Earthquake Engineering,* **47** (1), 15-27, 2014.

[9] E. Watanabe, K. Sugiura, W.O. Oyawa. Effects of multi-directional displacement paths on the cyclic behaviour of rectangular hollow steel columns. *Structural Engineering/Earthquake Engineering,* **17** (1), 69-85, 2000.

[10] American Concrete Institute. American Concrete Institute, Michigan, USA, 2008.

[11] Standards New Zealand, in *Part 5: Earthquake actions - New Zealand*. Wellington, New Zealand, 2004.

[12] J. Stanton, W.C. Stone, G.S. Cheok. A hybrid reinforced precast frame for seismic regions. *PCI journal,* **42** (2), 20-32, 1997.

[13] M. Priestley, G. Calvi, M. Kowalsky, Direct displacement-based seismic design of structures. Paper presented at the 5th New Zealand Society for Earthquake Engineering Conference. Palmerston North, New Zealand, 30 March-1 April 2007.

[14] D.J. Marriott, The development of high-performance post-tensioned rocking systems for the seismic design of structures. Ph.D. Dissertation, University of Canterbury Christchurch (2009).

Appendix A - Schematic drawing, test setup, and components

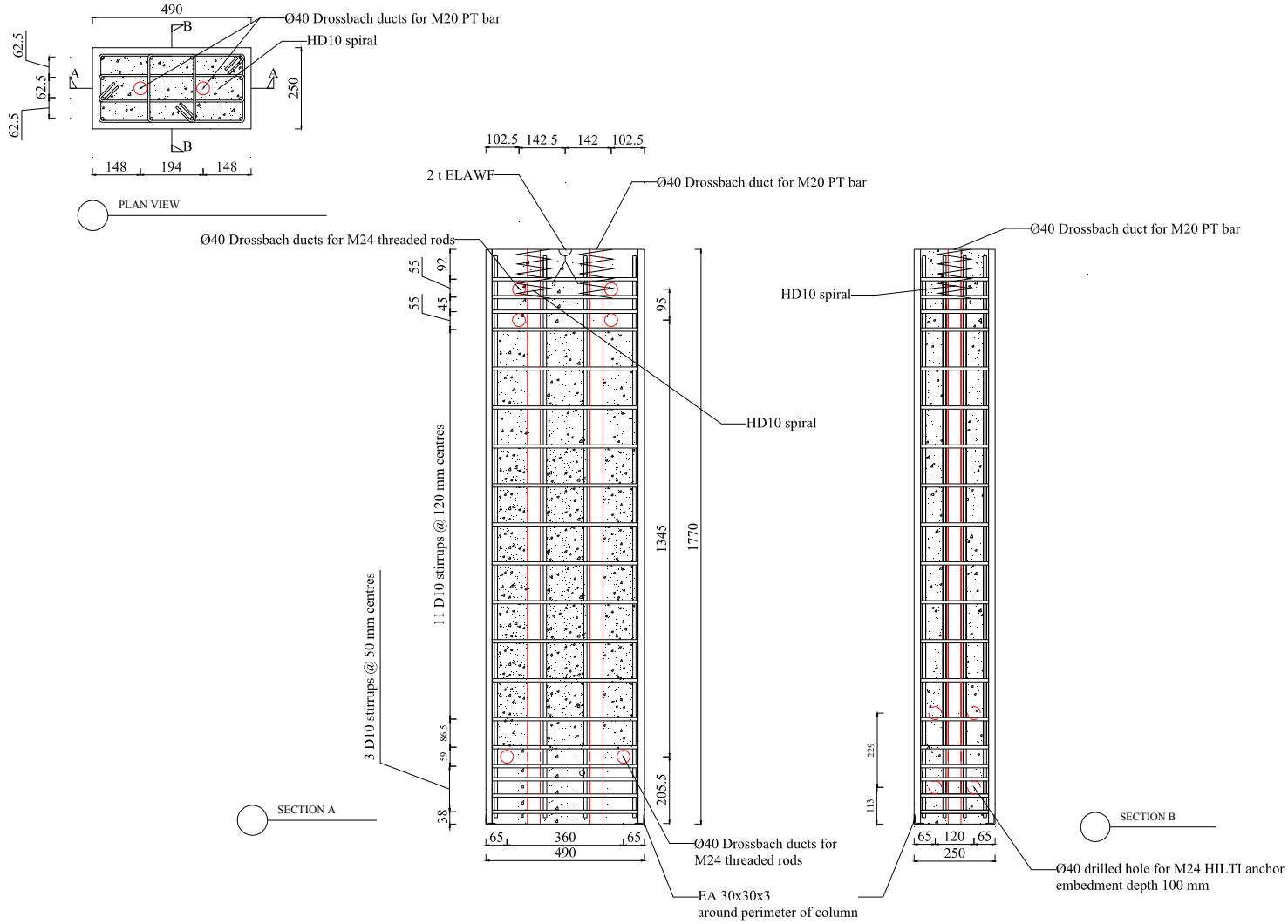

Figure A-1 Schematic drawing of column specimen

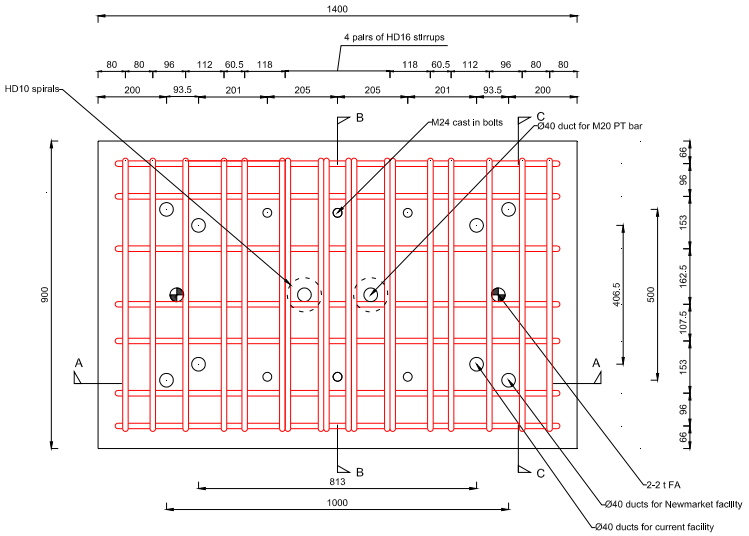

a) Plan view

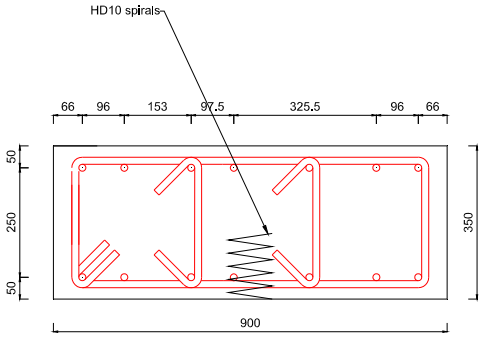

c) Section B-B

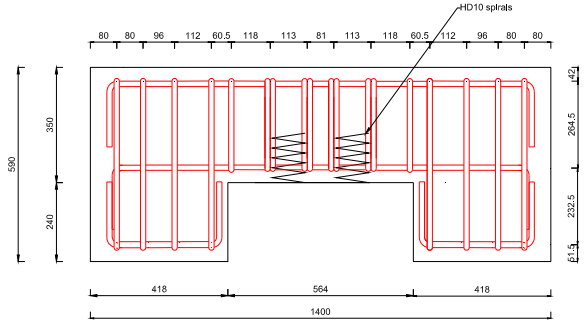

b) Section A-A

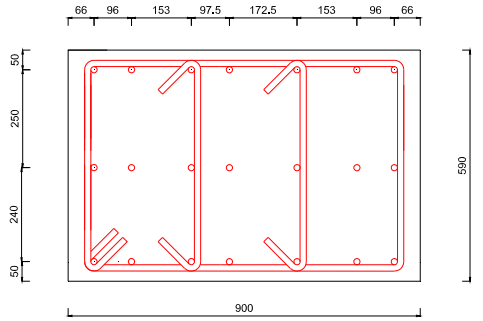

d) Section C-C

Figure A-2 Schematic drawing of foundation block

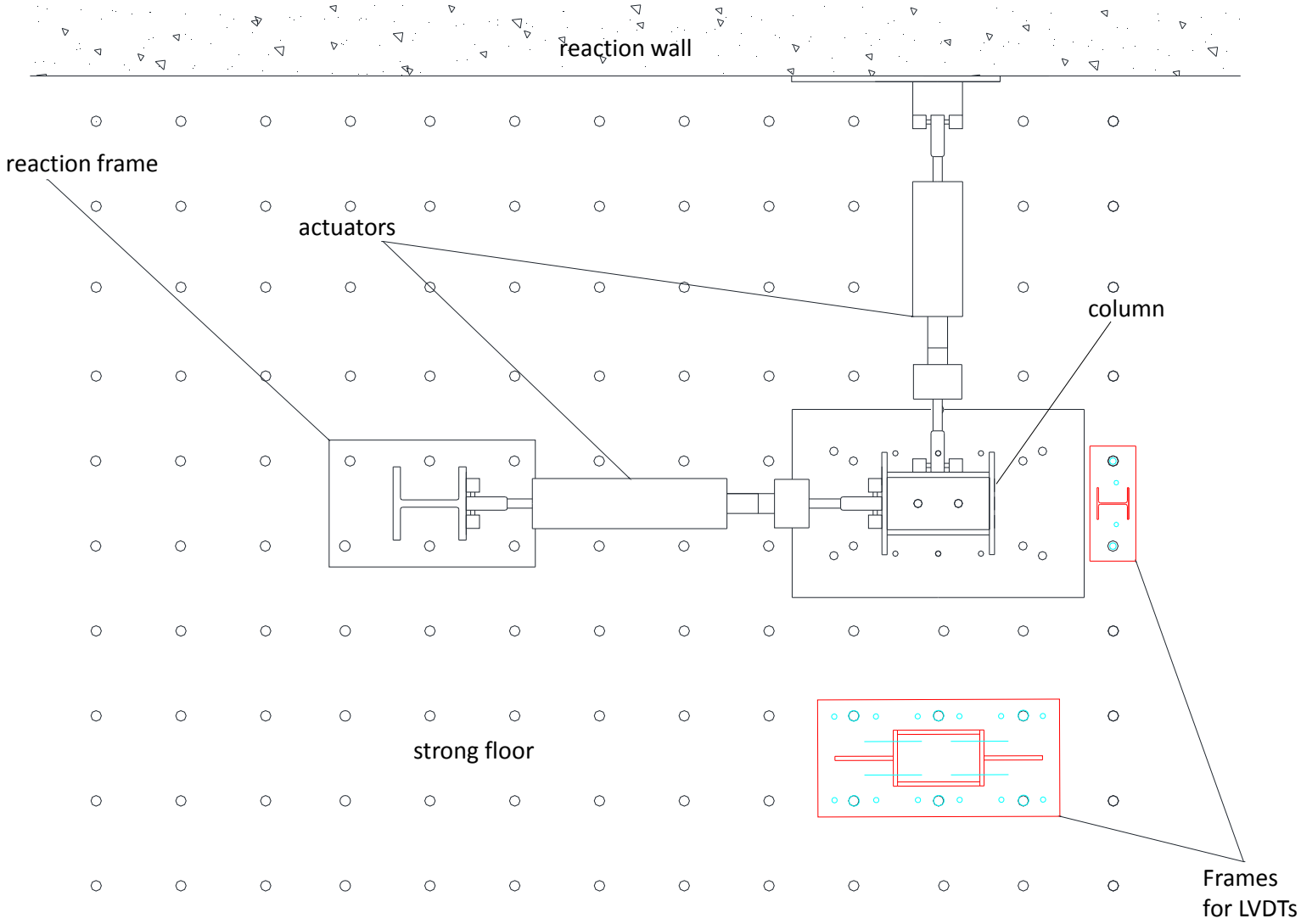

Figure A-3 Plan view of test setup

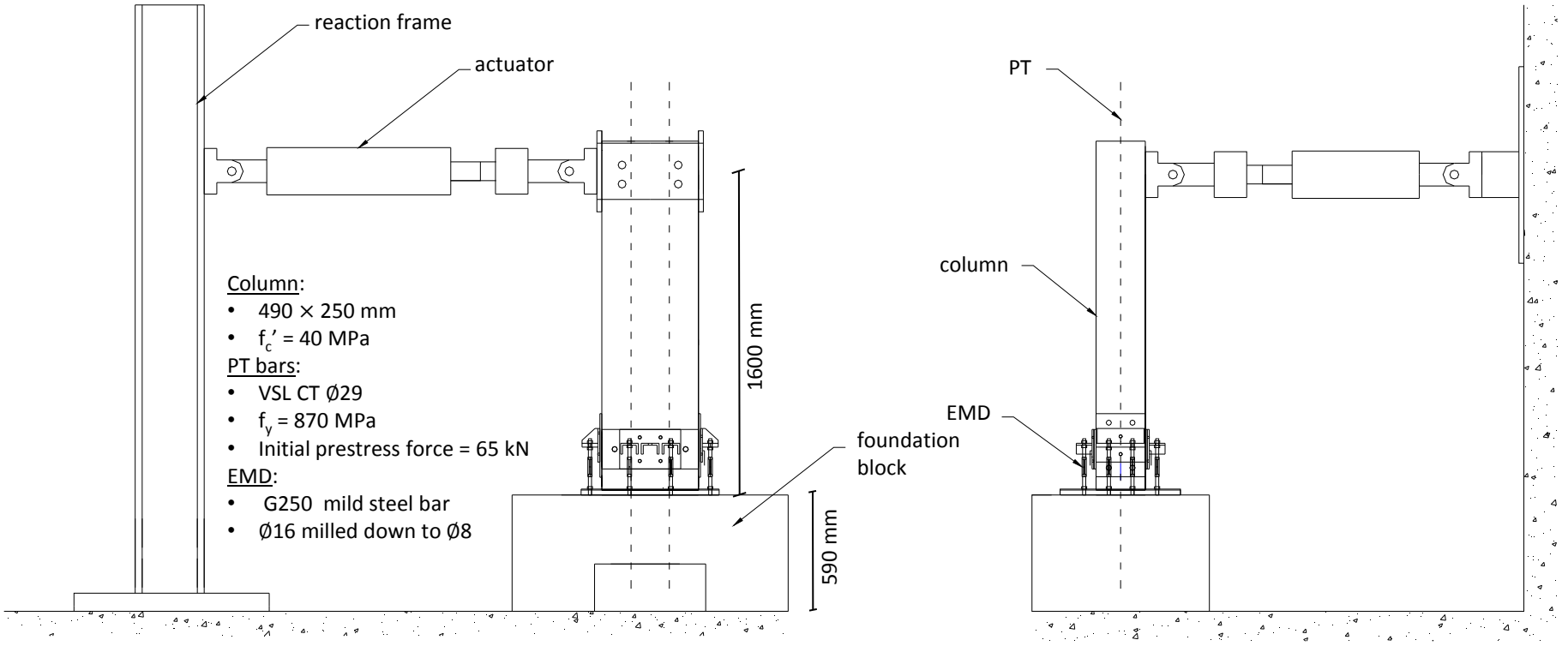

a) X- axis-face

b) Y- axis-face

Figure A-4 Elevation view of test setup

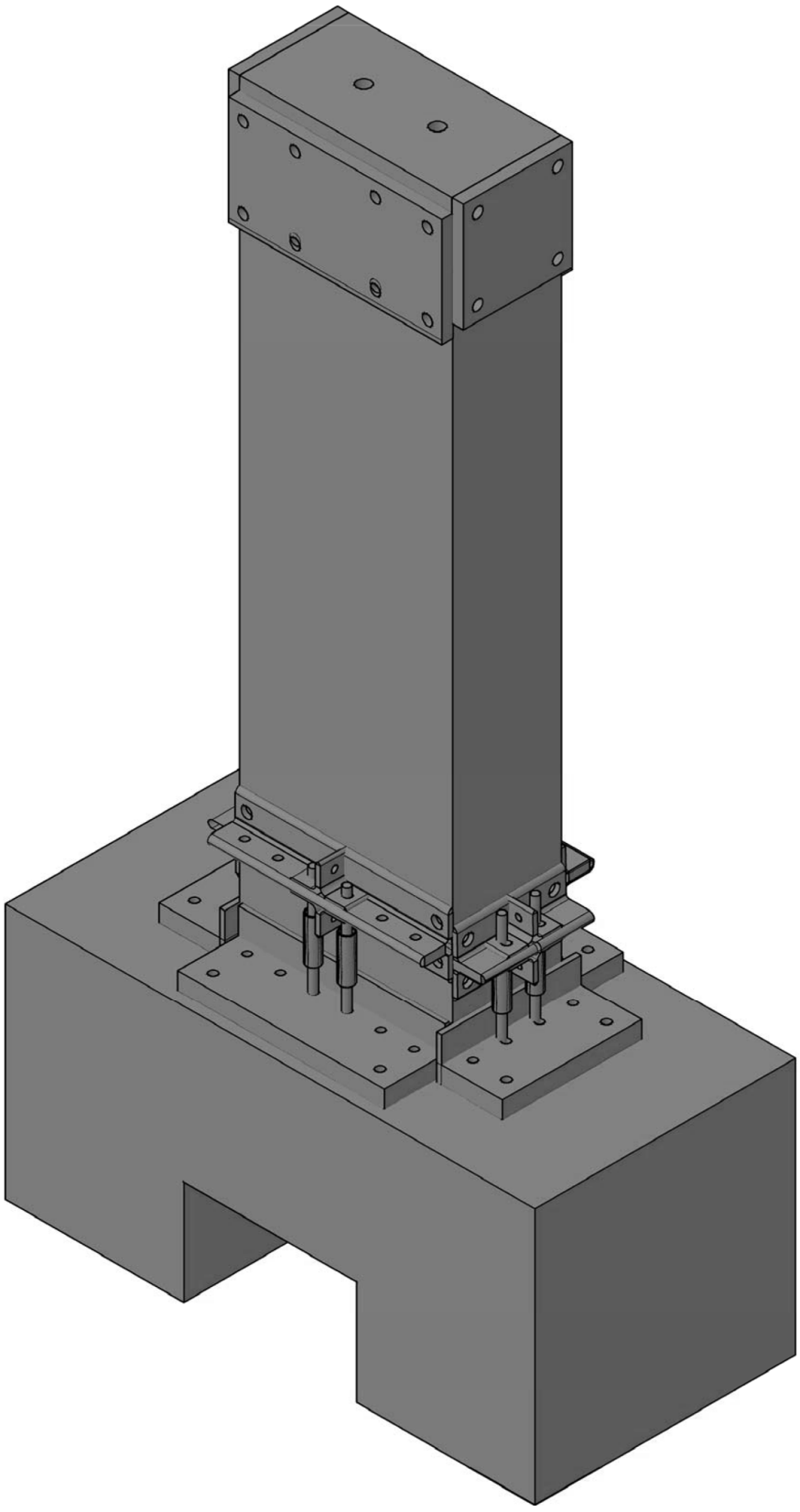

Figure A-5 Schematic of the column with steel base plate, EMD and actuator mounts.

a) Application of strain gauge

b) Epoxy injection

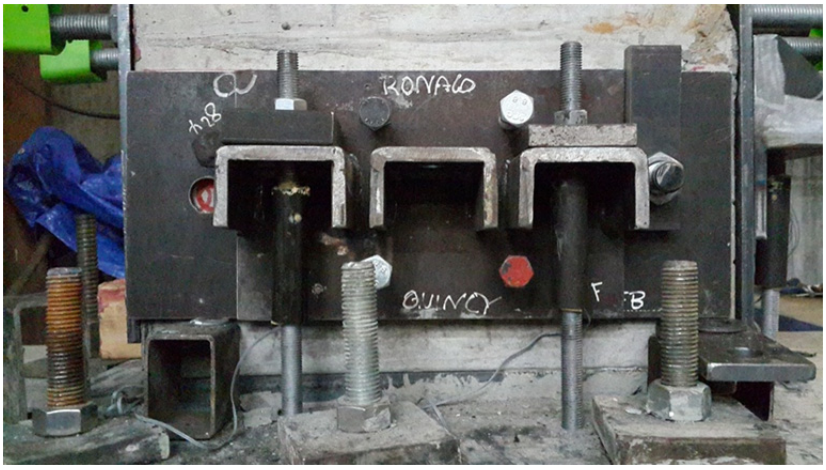

c) Mounting at the base of column using steel bracket

Figure A-6 Externally mounted dissipator (EMD)

Department of Civil & Environmental Engineering
Faculty of Engineering
The University of Auckland
Private Bag 92019 AMC
Auckland 1142, New Zealand

+64 9 373 7599
cee-enquiries@auckland.ac.nz